kexB Gene Correlates With *Aspergillus flavus* Keratitis Severity: A Whole-Genome Analysis

Jiamin Liu, Min Kang, Yuan Wei, Zijun Zhang, Jinding Pang, Qiankun Chen, Xizhan Xu, Zhenyu Wei, Yang Zhang, Kexin Chen, Zhiqun Wang, Xinxin Lu, and Qingfeng Liang

Beijing Institute of Ophthalmology, Beijing Tongren Eye Center, Beijing Tongren Hospital, Capital Medical University, Beijing Key Laboratory of Ophthalmology and Visual Sciences, Beijing, China

Correspondence: Qingfeng Liang, Beijing Institute of Ophthalmology, Beijing Tongren Eye Center, Beijing Tongren Hospital, Capital Medical University, Beijing Key Laboratory of Ophthalmology and Visual Sciences, 17 Hou Gou Lane, Chongwenmen Nei Street, Beijing 100005, China; lqflucky@163.com.

Received: November 21, 2024
Accepted: January 23, 2025
Published: February 14, 2025

Citation: Liu J, Kang M, Wei Y, et al. *kexB* gene correlates with *Aspergillus flavus* keratitis severity: A whole-genome analysis. *Invest Ophthalmol Vis Sci.* 2025;66(2):42. https://doi.org/10.1167/iovs.66.2.42

Purpose. Fungal keratitis caused by *Aspergillus flavus* (*A. flavus*) can result in severe inflammation and corneal stromal melting, leading to visual impairment. This study aimed to identify virulent genes correlated with the severity of *A. flavus* keratitis using whole-genome sequencing.

Methods. Whole-genome sequencing of 21 clinical *A. flavus* strains from cornea was performed to elucidate the pathogenesis of *A. flavus* in infectious keratitis, followed by pan-genome analysis and virulence analysis. To further understand the results from the previous analyses, growth phenotypes and virulence effect of mutant strains were validated experimentally, including the spore counting, growth pattern under different conditions, and clinical and pathological evaluation of *A. flavus* keratitis in mice models.

Results. The *A. flavus* pan-genome was composed of 17,326 gene clusters with a core genome of 5378 (31.0% of the pan-genome) orthogroups in all 21 isolates. Virulence gene analysis revealed 183 genes contributing to *A. flavus* pathogenesis and mutation of the *kexB* gene was associated with the severity of keratitis. The *kexB* mutant (Δ*kexB*) strains showed significantly reduced conidia formation and lower growth rates in the presence of the cell-wall perturbing agents. Further, the mice models validated that clinical score, and corneal perforation rates significantly decreased in the group infected by Δ*kexB* strains. Infiltration of immune cells, gene expression of cytokines, and matrix metalloproteinase (MMP) were also decreased in the mutant group.

Conclusions. The role of *kexB* gene in *A. flavus* keratitis was identified through whole-genome sequencing. Its mutation impairs conidia formation, cell wall integrity, and invasion, leading to milder clinical symptoms.

Keywords: *aspergillus flavus* (*A. flavus*), fungal keratitis, whole genome sequencing, *kexB*, cell wall integrity, prognosis, immune response

Fungal keratitis annually afflicts millions of people globally, with 10% of cases culminating in eye removal due to delayed diagnosis or suboptimal therapeutic outcomes.[1] Typically, the infection occurs when environmental pathogens invade the cornea via a wound subsequent to corneal trauma. *Aspergillus* species, with their ubiquitous airborne conidia, are significant causative agents, particularly in tropical regions.[2] Among them, *Aspergillus flavus* (*A. flavus*), as one of the most commonly isolated pathogens in fungal infection, is estimated to constitute 75% of keratitis cases within the *Aspergillus* genus owing to its invasive propensity and production of mycotoxins.[3,4] The potent pathogenicity and rapid disease advancement of *A. flavus* can lead to severe vision impairment or even blindness without prompt diagnosis and treatment.[5] Our previous study had indicated that the incidence of *Aspergillus* keratitis has been steadily ascending in recent years, imposing a substantial burden on individuals and society.[6]

The host immune status is of paramount importance for the prognosis of *A. flavus* keratitis. Concurrently, genetic and phenotypic variations among strains also exert a considerable influence.[7,8] Factors such as thermotolerance, secondary metabolites, cell wall integrity, stress response, and transcription act as determinants of virulence in both plant and animal models.[9–12] Additionally, Barakat et al. found that AFB1 toxin–encoding gene was detected in more than half of the isolates, and there was a significant correlation between severity of keratitis and the quantity of aflatoxin B1 production.[13] These findings underscore the connection between strain-level genetics and clinical severity, highlighting the necessity for further investigation into the pathogen features isolated from patients.

Pan-genome analysis, which centers on comprehensive genetic diversity by utilizing multiple isolates rather than a single strain, has emerged as an effective approach to capture the extensive diversity within a species and conduct in-depth investigation on novel gene clusters and their regulation. Amelia et al. identified genomic variation associated with clinical isolates and triazole resistance and character-

ized genetic variation in known virulence factors through *A. fumigatus* pan-genome analysis.[8] Gangurde et al. provided a complete pangenome framework for *A. flavus* in agricultural environments along with associated genes for pathogen survival and aflatoxin production.[14] However, research into the specific pathogenic mechanisms of *A. flavus* in corneal infections, particularly the exploration from the genomic level, remains relatively scarce.

This study is designed to provide insights into the relationship between genomic characteristics and clinical features by analyzing clinical cases of *A. flavus* keratitis and exploring the genomic features of isolated pathogens. Additionally, we aim to identify virulent genes correlated with the prognosis of patients, thereby facilitating the development of more effective diagnostic methods and prediction of the outcomes of *A. flavus* keratitis.

Materials and Methods

Establishment of *A. flavus* Keratitis Cohort

Twenty-one consecutive patients (21 eyes) with *A. flavus* keratitis were included in the study, from the Department of Ophthalmology at Beijing Tongren Hospital, Capital Medical University, between 2019 and 2023. The inclusion criteria were as follows: patients had typical clinical manifestations of *A. flavus* keratitis and at least one positive etiological examination (corneal scraping and microbial culture). The data encompassed demographic details, time of presentation, predisposing factors, anterior segment photography, administered treatments, and outcomes. Based on the corneal ulcer scoring system, the severity of patients with *Aspergillus* keratitis was graded as mild, moderate, and severe.[15] The study was conducted in accordance with the Declaration of Helsinki and was approved by the Medical Ethics Committee (TRECKY2021–024).

Fungal Strains and Growth Conditions

The conidia of 21 strains of *A. flavus* isolated from corneal scrapings between 2019 and 2023 were stored at −80°C in an ultra-freezer in 25% to 50% (v/v) glycerol for long-term preservation. *A. flavus* ATCC 204304 served as the quality control strain in this study. These strains were inoculated on potato glucose agar (PDA; Dijing, Guangzhou, China) and cultured at 28°C for at least 3 days. Subsequently, the conidia were collected and resuspended in saline with 0.1% Tween to the desired concentration. The spore titers were determined using a hemocytometer.

Antimicrobial Susceptibility Testing

To perform the antimicrobial susceptibility testing, 100 µL conidial suspensions were diluted with 10 mL of RPMI-1640 medium (DL Biotech, Zhuhai, China) for the final inoculum density (0.4×10^4 to 5×10^4 CFU/mL).[16,17] Then 100 µL of the suspension was added into each well of a 96-well plate, which was combined with lyophilized antifungal drugs (Terbinafine, Natamycin, Voriconazole, Posaconazole, Itraconazole, and Amphotericin B; DL Biotech, Zhuhai, China). The plates were sealed and incubated at 35°C for 48 hours.[18–20] Resistance was defined according to the clinical breakpoints established by European Committee on Antimicrobial Susceptibility Testing (EUCAST).

Whole Genome Sequencing and Annotation

Genomic DNA (gDNA) was extracted from each strain using the Quick-DNA fungal/bacterial miniprep kit (Zymo Research) according to the manufacturer's protocol. The concentration and purity of the gDNA samples were evaluated using Nanodrop2000 (Thermo Fisher Scientific, Waltham, MA, USA). Subsequently, the gDNA samples were submitted for whole genome sequencing (WGS) on the Illumina Novaseq platform in the PE150 mode (Novogene, Tianjin, China). The raw data obtained from the WGS were filtered to eliminate low-quality data, including reads containing low-quality bases (>40%), reads containing >10% N, and reads with an overlap between adapters exceeding 15 bp.

De Novo Genome Assembly and Annotation

Genomes were assembled de novo by SPAdes version 3.15.5 with the reference genome (ASM1411746) as a guide. The quality of the genome assembly was assessed using QUAST version 5.0.2. Contigs that were shorter than 500 bp or possessing >95% identity and coverage overlap with other contigs were removed.[21] Gene prediction and functional annotation were performed using the Funannotate pipeline, which included MEROPS version 12,[22] dbCAN2 release 9.0,[23] BUSCO version 4.1.4.,[24] and InterProScan version 5.45–80.0.[25]

Pan-Genome Analysis and Phylogenetic Analysis

Pan-genome analysis, comprising core genes present in all individuals, accessory genes that are not shared between all members, and unique genes found in a single strain, was performed using BPGA version 4.6.6 (using default parameters and 50% sequence identity cutoff).[26] The phylogenetic tree based on the whole genome was constructed using iTOL (https://itol.embl.de). Further analysis of the gene accumulation curve and core-unique sequence composition was based on these results. Additionally, clusters of orthologous groups (COGs) functional enrichment of the predicted proteins were performed.[27]

Analysis of Virulence Genes

The protein sequences of 21 genomes were aligned using DIAMOND,[28] adhering to the following criteria: a cutoff of 40% identity, 70% coverage, and an E value of 1e-10 against the Pathogen Host Interactions Database (PHI).[29] Based on the specific distribution and presence of certain virulence genes, the 21 strains of *A. flavus* isolated from the cornea were presented using R software version 4.2.2 (The R Foundation, Vienna, Austria). STRING version 11.0 was used to analyze interactions between potential virulence gene and the predicted functional partners.[30]

Experimental Validation of Virulence Genes for Corneal Pathogenicity

Phenotyping of Isolates. Each isolate was cultivated in PDA for 5 days at 28°C, and 1 µL conidia suspension (containing 10^5 spores) of each strain was inoculated into PDA media, respectively. After incubation for 5 days at 28°C, conidia were resuspended in saline containing 0.1% Tween-20 and counted under microscopy using a hemocytome-

Investigative Ophthalmology & Visual Science

ter. For stress resistance analysis, the conidia were spotted on PDA media supplemented with cell-wall perturbing agent (100 µg/mL Congo red) or osmotic stress agent (1 mmol/L NaCl). All plates were incubated in the dark at 28°C for 5 days and the diameter of each colony was recorded.

Mice Model of *A. flavus* Keratitis. Thirty C57BL/6N mice aged 6 to 8 weeks, with an equal number of males and females were purchased from Vital River Laboratory Animal Technology Co., Ltd. (Beijing, China) and maintained in a pathogen-free environment for 1 week. Subsequently, they were randomly divided into three groups: the control group (receiving an injection of phosphate-buffered solution into the corneal stroma), the mutant group (corneal infection with spore suspension from the mutant strains), and the wild-type (WT) group (corneal infection with spore suspension from the WT strains). Specifically, after the mice were anesthetized with an intraperitoneal injection of 0.1% sodium pentobarbital (Sigma, USA), 1 µL conidia suspension (containing 105 spores) or sterile PBS was injected into the central corneal stroma of the left eyes using a 33-gauge syringe (Hamilton 21-2062).[31] Only the left eye of each mouse was utilized for the experiments. The right eye of each mice model was set as absolute control and remained intact throughout the animal experiments.

Corneal Examination and Scoring. The models with *A. flavus* keratitis were evaluated using a slit lamp microscope (Topcon SL-D7, Tokyo, Japan) on day 1, day 3, and day 5 ($n = 4$/group/time). Additionally, 1% sodium fluorescein (Shanghai Yuanye Bio-Technology Co., Ltd., China) was instilled into the inferior conjunctival sac of the mice, and the corneal staining patterns were photographed with a cobalt blue filter. The corneal opacity was assessed using a corneal scale that encompassed 3 criteria: opacity area, opacity density, and surface regularity, with each criterion being graded on a scale from 0 to 4.[32] A total score of 0 was given for a normal cornea and 12 for the worst cornea.

Tissue Collection. On day 3 after infection, the mice were euthanized ($n = 6$/group/time). Subsequently, the corneas were meticulously removed and half stored at −80°C in the refrigerator, with half in 4% paraformaldehyde (for paraffin sections) for further experiments.

RNA Extraction and RT-qPCR. Total RNA was extracted from the corneas using the RNA Easy Fast Tissue/Cell Kit (Tiangen, Beijing, China). Then, the RNA was reversed transcribed (RT) to cDNA using the HiScript III All-in-One RT SuperMix (Vazyme, Nanjing, China). Real-time quantitative polymerase chain reaction (RT-qPCR) was performed using Tag Pro Universal SYBR qPCR Master Mix (Vazyme, Nanjing, China) on an ABI 7500 system (Applied Biosystems, USA). The qPCR procedure consisted of an initial step at 95°C for 30 seconds, followed by 40 cycles of denaturation at 95°C for 10 seconds, and annealing and extension at 60°C for 30 seconds. Three corneas in each group were used for real-time PCR and the relative expression of the mRNA was calculated using the $2^{-\Delta\Delta Ct}$ method. Mice β-actin expression acted as an endogenous reference to normalize relative gene expression. Primer sets used in qRT-PCR are listed in Supplementary Table S1.

Hematoxylin and Eosin Staining. After deparaffinization and hydration, the corneal paraffin sections were incubated with hematoxylin for 5 minutes and 0.5% acid alcohol differentiation solution for 5 seconds, then washed with tap water for 3 minutes. Thereafter, they were stained with eosin for 30 seconds.

Immunohistochemistry Staining. For immunohistochemistry (IHC) staining, corneal paraffin sections were deparaffinized twice with xylene for 10 minutes each and hydrated with gradient alcohol. Then, the heat-mediated antigen retrieval was conducted. Endogenous peroxidase was blocked by 3% hydrogen peroxide for 10 minutes. After being permeabilized with 0.1% Triton X-100 for 20 minutes and blocked with goat serum for 1 hour at room temperature, the paraffin sections were incubated with anti-TNF alpha (1:250; ab1793, Abcam), anti-IFN-γ (1:200, bs-0480R, Bioss), anti-MMP13 (1:200; 18165-1-AP, proteintech), anti-MMP3 (1:50; ab52915, Abcam), anti-MPO antibodies (1:200; 22225-1-AP, proteintech), CD68 antibody (1:250; sc-70761, Santa Cruz Biotechnology), or CD3 antibody (1:150; ab16669, Abcam) overnight at 4°C. Subsequently, the sections were washed and incubated with goat anti-rabbit IgG H&L (1:1000, ab205718; Abcam) or goat anti-mouse IgG H&L (HRP; 1:1000, ab205719; Abcam) for 1 hour at room temperature. Finally, they were stained with DAB (ZSGB-BIO, Beijing, China) for 5 to 10 minutes and observed under a microscope with 400-fold magnification. The cells with brown-stained cytoplasm were considered positive.

Statistical Analysis

Statistical analyses were conducted using Prism software (version 9.0; GraphPad Software Inc., San Diego, CA, USA). Continuous data between the two groups were analyzed by *t*-test or Mann-Whitney *U* test, whereas among the three groups, the 1-way ANOVA or Kruskal-Wallis test was used. Categorical variables were analyzed by Chi-square test or Fisher exact test. All the hypotheses tested were 2-tailed, and $P < 0.05$ was considered statistically significant.

Results

Clinical Manifestations

A total of 21 patients presenting with *A. flavus* keratitis during 2019 to 2023 were included. The median age was 50.4 ± 13.5 years (range from 26 to 65 years) and 61.9% (13 of 21) of the patients were men. All of them had unilateral infections. The risk factors associated with *A. flavus* keratitis were shown in Table 1. Among these cases, 9 of the 21 patients (42.9%) had a history of trauma, 1 patient had a history of long-term dry eye and diabetes, and 1 had a history of corneal surgery. The average duration from the onset of symptoms to arrival at our hospital was 21.2 ± 12.9 days, ranging from 5 to 45 days. At the initial visit, 8 patients presented with moderate (8 of 21) symptoms and 13 had severe symptoms based on the severity scale. After medical treatment, 4 (19.0%) patients showed improvement in clinical manifestations, whereas 17 of 21 (81.0%) required keratoplasty.

The minimum inhibitory concentrations (MIC) results (Table 2) demonstrated that the most effective drugs for *A. flavus* isolates were Posaconazole (0.06–0.125 µg/mL, MIC_{50} = MIC_{90} = 0.06 µg/mL), Itraconazole (0.06–0.125 µg/mL, MIC_{50} = MIC_{90} = 0.125 µg/mL), and Terbinafine (0.06–0.125 µg/mL, MIC_{50} = MIC_{90} = 0.125 µg/mL), followed by Voriconazole (0.125–0.5 µg/mL, MIC_{50} = MIC_{90} = 0.25 µg/mL), and then Amphotericin B (0.5–1 µg/mL, MIC_{50} = MIC_{90} = 0.5 µg/mL). For the same isolates, Natamycin (32–128 µg/mL, MIC_{50} = 32 µg/mL and MIC_{90} = 64 µg/mL) was found to be the least effective. The MIC of strains

Investigative Ophthalmology & Visual Science

Table 1. Clinical and Genomic Features of 21 Patients With *Aspergillus* Keratitis

Patient Number	Gender	Age	Risk Factors	Onset Time, D	Severity	Prognosis	Strain	Total Length, M	No. of Contigs, ≥5000 bp	GC, %	Gene Number
1	F	43	NA	NA	Severe	Poor	Asp1117	37.30	133	47.62	11939
2	F	63	NA	NA	Severe	Poor	Asp1318	37.00	101	48.09	12768
3	M	40	Trauma	28	Severe	Poor	Asp1352	37.26	106	47.97	12338
4	M	27	Trauma	10	Moderate	Poor	Asp1373	37.01	154	48.13	12709
5	M	53	NA	NA	Severe	Poor	Asp1398	36.89	128	48.09	12308
6	M	40	Trauma	34	Severe	Poor	Asp1402	37.80	125	47.66	12096
7	F	42	Trauma	20	Moderate	Poor	Asp1614	37.36	145	47.62	12605
8	F	42	Trauma	6	Moderate	Good	Asp1672	37.46	122	47.84	12446
9	M	65	Trauma	23	Severe	Poor	Asp1784	42.47	391	49.47	16101
10	M	61	Trauma	7	Severe	Poor	Asp1789	38.74	150	47.49	13231
11	F	57	None	5	Moderate	Good	Asp1887	37.23	121	48.17	12658
12	M	53	Trauma	45	Severe	Poor	Asp1930	37.91	93	47.37	12352
13	M	39	None	14	Moderate	Good	Asp1967	39.16	815	48.10	13020
14	F	50	None	40	Severe	Poor	Asp2343	38.02	218	47.84	12942
15	M	49	NA	NA	Severe	Poor	Asp2371	37.81	166	47.28	12077
16	M	49	NA	NA	Severe	Poor	Asp2385	39.51	127	48.53	14522
17	M	63	Trauma	39	Severe	Poor	Asp2428	37.06	153	48.16	13084
18	M	60	NA	NA	Moderate	Poor	Asp2436	37.66	162	47.19	12235
19	M	63	None	20	Moderate	Good	Asp2458	37.06	119	47.79	11167
20	F	49	Dry eyes, diabetes	7	Severe	Poor	Asp2601	37.31	128	47.81	12053
21	F	26	Corneal surgery	20	Moderate	Poor	Asp2799	37.52	135	47.51	12230

Table 2. Antifungal MIC Values of *A. flavus* Strains Isolated From Corneal Ulcers

Strain	Terbinafine, µg/mL	Natamycin, µg/mL	Voriconazole, µg/mL	Posaconazole, µg/mL	Itraconazole, µg/mL	Amphotericin B, µg/mL
Asp1117	0.06	32	0.25	0.06	0.06	0.5
Asp1318	0.125	32	0.5	0.125	0.125	0.5
Asp1352	0.06	32	0.125	0.06	0.06	0.5
Asp1373	0.06	32	0.25	0.06	0.06	0.5
Asp1398	0.06	32	0.125	0.06	0.125	0.5
Asp1402	0.125	32	0.25	0.06	0.125	0.5
Asp1614	0.06	32	0.125	0.06	0.06	0.5
Asp1672	0.125	64	0.5	0.125	0.125	0.5
Asp1784	0.06	64	0.125	0.06	0.06	0.5
Asp1789	0.125	32	0.125	0.06	0.06	0.5
Asp1887	0.06	32	0.125	0.06	0.06	0.5
Asp1930	0.125	32	0.125	0.06	0.06	0.5
Asp1967	0.06	32	0.125	0.06	0.06	0.5
Asp2343	0.125	64	0.25	0.06	0.125	0.5
Asp2371	0.125	64	0.25	0.06	0.125	0.5
Asp2385	0.125	32	0.25	0.06	0.125	0.5
Asp2428	0.125	64	0.25	0.06	0.125	0.5
Asp2436	0.06	32	0.25	0.06	0.06	0.5
Asp2458	0.125	64	0.25	0.06	0.125	1
Asp2601	0.125	32	0.25	0.06	0.125	0.5
Asp2799	0.125	128	0.25	0.06	0.125	1

isolated from different outcomes was compared. However, there was no significant difference between the MIC and prognosis.

Whole-Genome Analysis Showed Functional Differences of Two Groups

General Genomic Features and Whole-Genome Phylogenetic Analysis. The high-quality data of 21 isolates of *A. flavus* were sequenced and assembled. FastQC and Trimmomatic were used to control the raw data for an average quality, and reads of low quality were excluded. The main obtained genomic characteristics and annotation information are presented in Table 1. The average genome size was 37.9 Mb (range from 36.8 to 42.4 Mb), with 47.9% of the GC content on average. The mean gene number was 12709, ranging from 11167 to 16101. To further investigate the inter-relationship among the strains, a phylogenetic tree was constructed based on the whole genome. In addition, the clinical prognoses of patients infected by these 21 *A. flavus* strains were incorporated around the circular whole-genome phylogenetic tree (Fig. 1). Upon meticulous analysis of the phylogenetic tree, it was revealed that these strains, despite eliciting disparate prognoses in patients,

Investigative Ophthalmology & Visual Science

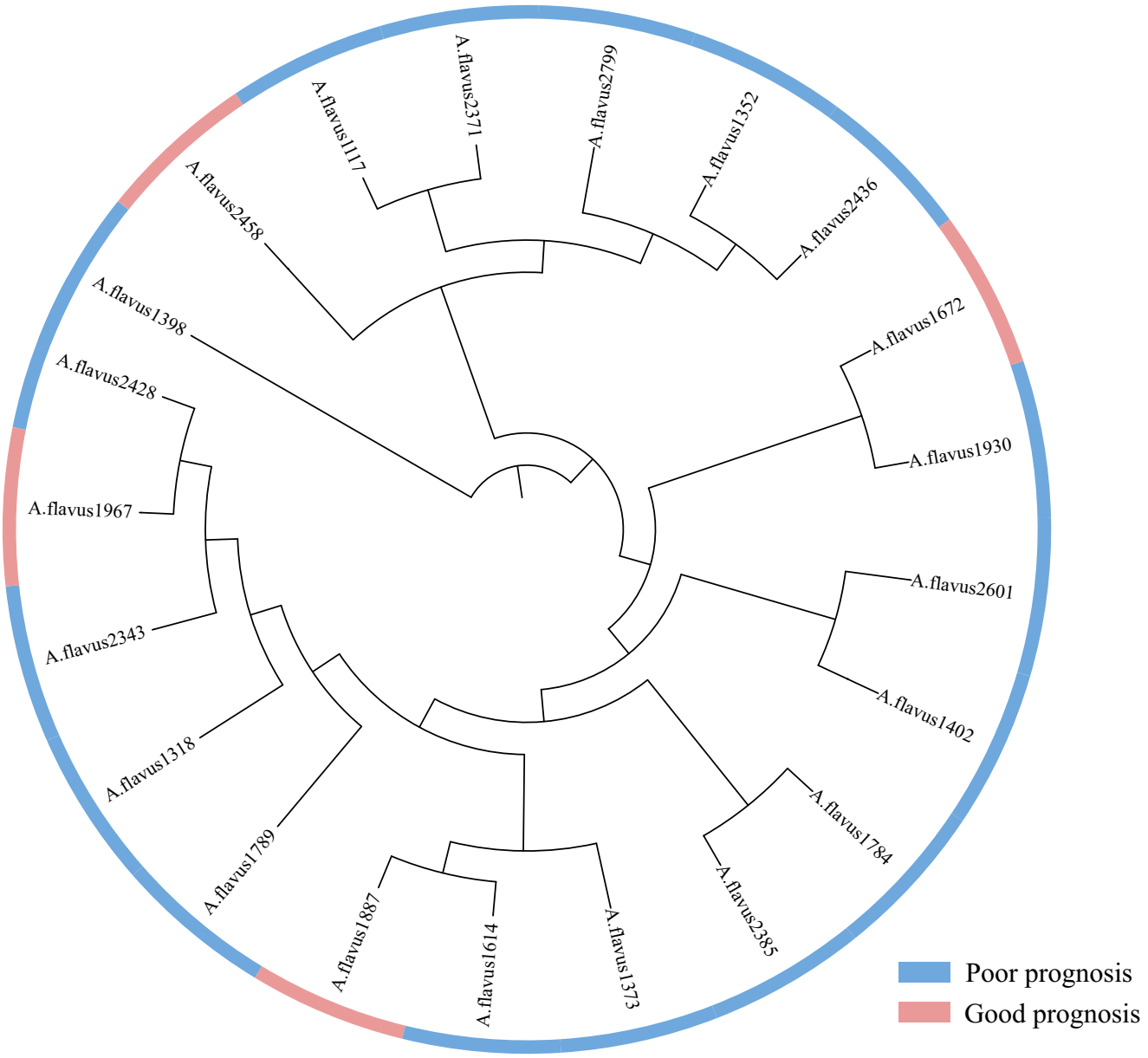

Figure 1. Whole-genome phylogenetic analysis of 21 *A. flavus* strains. The *colored ring* shows the clinical prognoses of patients infected by these strains.

did not exhibit significant differences at the whole-genome level.

Pan-genomic and Functional Characterization of *A. flavus* Strains. Given the lack of research on the pan-genomic characteristics of *A. flavus*, the core and pan-genome were analyzed for the purpose of comparing the general genetic similarities and diversity among all the strains. Empirical power-law regression and exponential curve fitting were used for extrapolation of the pan- and core genome curves, respectively, as presented in Figure 2A. The number of pan-genomes did not substantially increase after the addition of approximately 20 genomes, indicating that the pan-genomes were in a "close" state. The *A. flavus* pan-genome was composed of 17,326 gene clusters with a core genome of 5378 (31.0% of the pan-genome) ortho groups in all 21 isolates. Furthermore, the detailed distribution of unique genes in each genome was exhibited (Fig. 2B), and the results showed that strain Asp1784 contained the largest number of unique genes ($n = 2428$), whereas strain Asp2799 had the smallest number of unique genes ($n = 10$). Among the COG of Proteins database categories, core genes were found to be significantly abundant in the general function prediction (21.5%). However, the unique genes were more enriched in cell wall/membrane/envelope biogenesis, cell motility, and transcription.

Based on the clinical prognosis, we grouped strains from different backgrounds for COG functional differences analysis (Fig. 2C). In terms of core genes, the COG functional analysis of the two groups showed no significant difference. However, 7 categories (D, M, Q, P, R, and S) of the accessory genome, and 13 categories (M, N, O, T, K, C, G, H, I, Q, P, R, and S) of the unique genome were

Investigative Ophthalmology & Visual Science

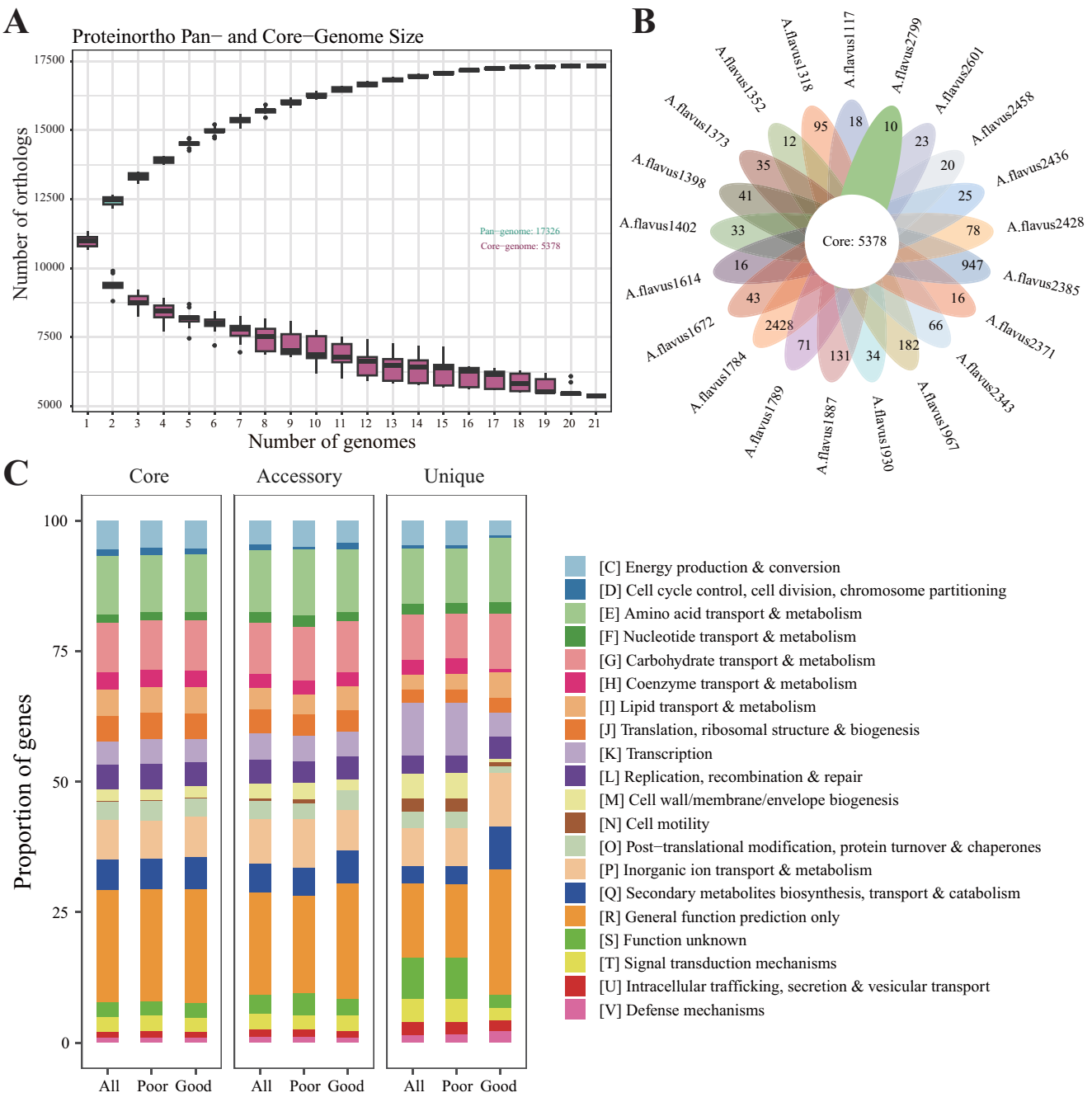

Figure 2. Pan-genome analysis of 21 *A. flavus* strains. (**A**) Genome size evolution curves of the pan-genome (*blue*) and core genome (*orange*) grouped. (**B**) The number of core genes among all strains and unique genes of individual strain. (**C**) The percentage (%) of COG categories and annotations of predicted genes within the core, accessory, and unique genomes of all strains, strains with poor and good prognosis.

observed with significant differences. Notably, categories M (cell wall/membrane/envelope biogenesis) and categories S (function unknown) of accessory and unique genomes were highly represented in strains with poor clinical prognosis, which may potentially play a pivotal role in the progression and prognosis of *A. flavus*.

Virulence-Related Genes in *A. flavus* Genomes. One hundred eighty-three virulence-associated genes were identified using the PHI database. This list includes genes involved in cell wall integrity (19 genes), initiation of germ tubes (2 genes), nutrient uptake in invasive growth (11 genes), resistance to host immune response (4 genes), response to stress (15 genes), toxins (9 genes), etc. Overall, the majority of virulence-associated factors were well conserved. 145 of 183 (79.2%) of the genes were present in all genomes. The remaining 38 virulence-associated genes had some degree of genetic variation expected to affect gene function among our 21 genomes, which can be visualized in Figure 3A. Among them, 31 genes were mutated in 4.8% of the isolates (1/21); 4 genes, including *Fcr3*, *kexB*,

Investigative Ophthalmology & Visual Science

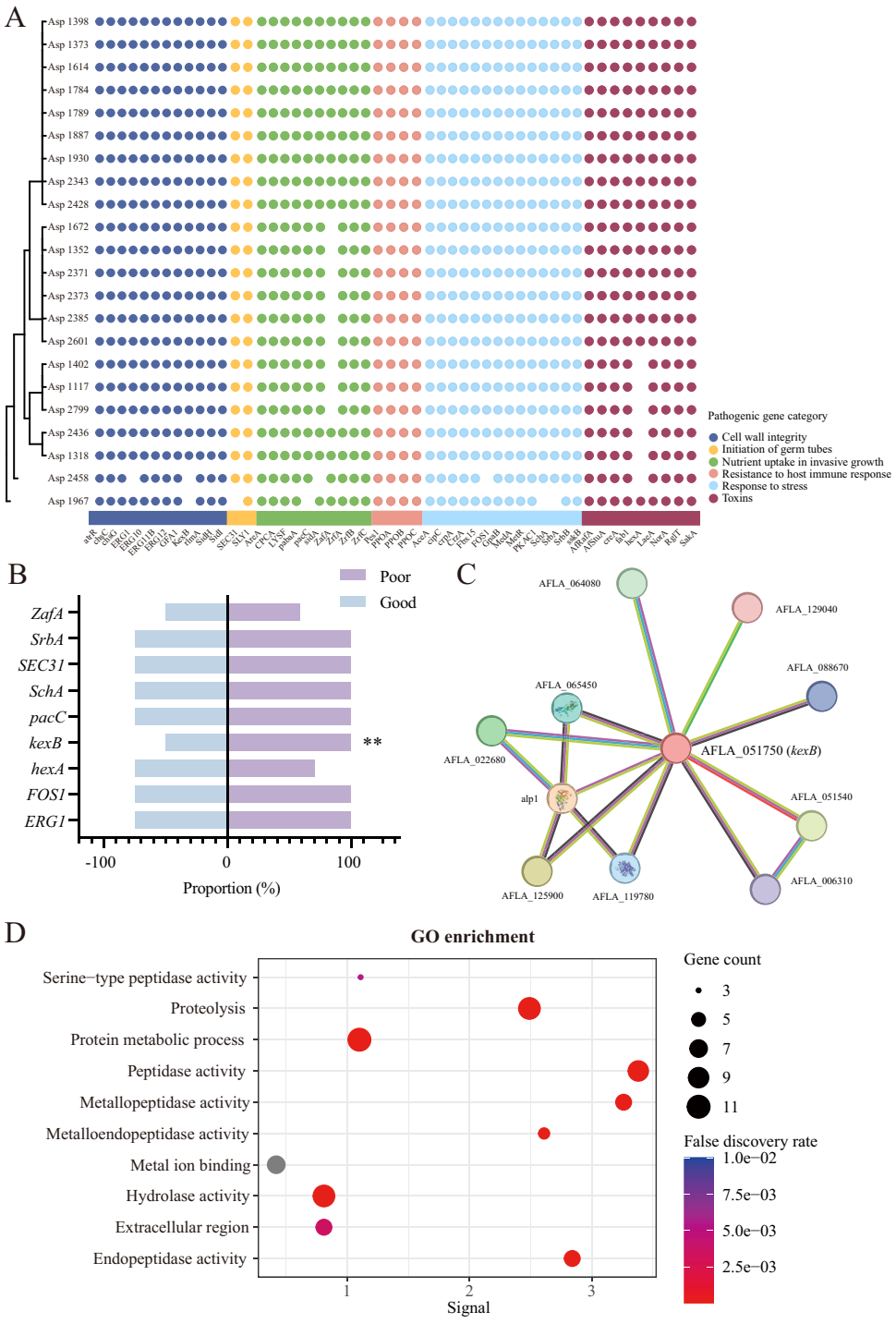

Figure 3. Virulence-related genes in *A. flavus* genomes. (**A**) Comparative analysis of virulence factor profiles across 21 *A. flavus* genomes. (**B**) The proportion of virulence gene mutations in groups with good and poor prognosis. (**C**) Interactions between *kexB* gene and the predicted functional partners. (**D**) GO functional enrichments in the *kexB* network. ****$P < 0.0001$, ***$P < 0.001$, **$P < 0.01$, *$P < 0.05$; ns, not significant.

HorA, and *tmpL*, were mutated in 9.5% of the genomes (2/21). Furthermore, we observed absence of *hexA* gene, encoding aflatoxin biosynthesis in 6 (28.6%) isolates and the *ZafA* gene, regulating zinc homeostasis in 9 (42.9%) strains. Compared with the proportion of gene mutant in the clinical good prognosis (2/4, 50%) and with poor prognosis (0/17), we found there was a significant difference in the *kexB* gene, a gene coding for kexin-like proteinases and affecting cell wall integrity between the two groups ($P = 0.002$; Fig. 3B). We then analyzed the interactions between the *kexB* gene and the predicted functional partners using Search Tool for the Retrieval of Interacting Genes (STRING; see Fig. 3C). Functional enrichments showed that the gene functions in *kexB* network were mainly enriched in

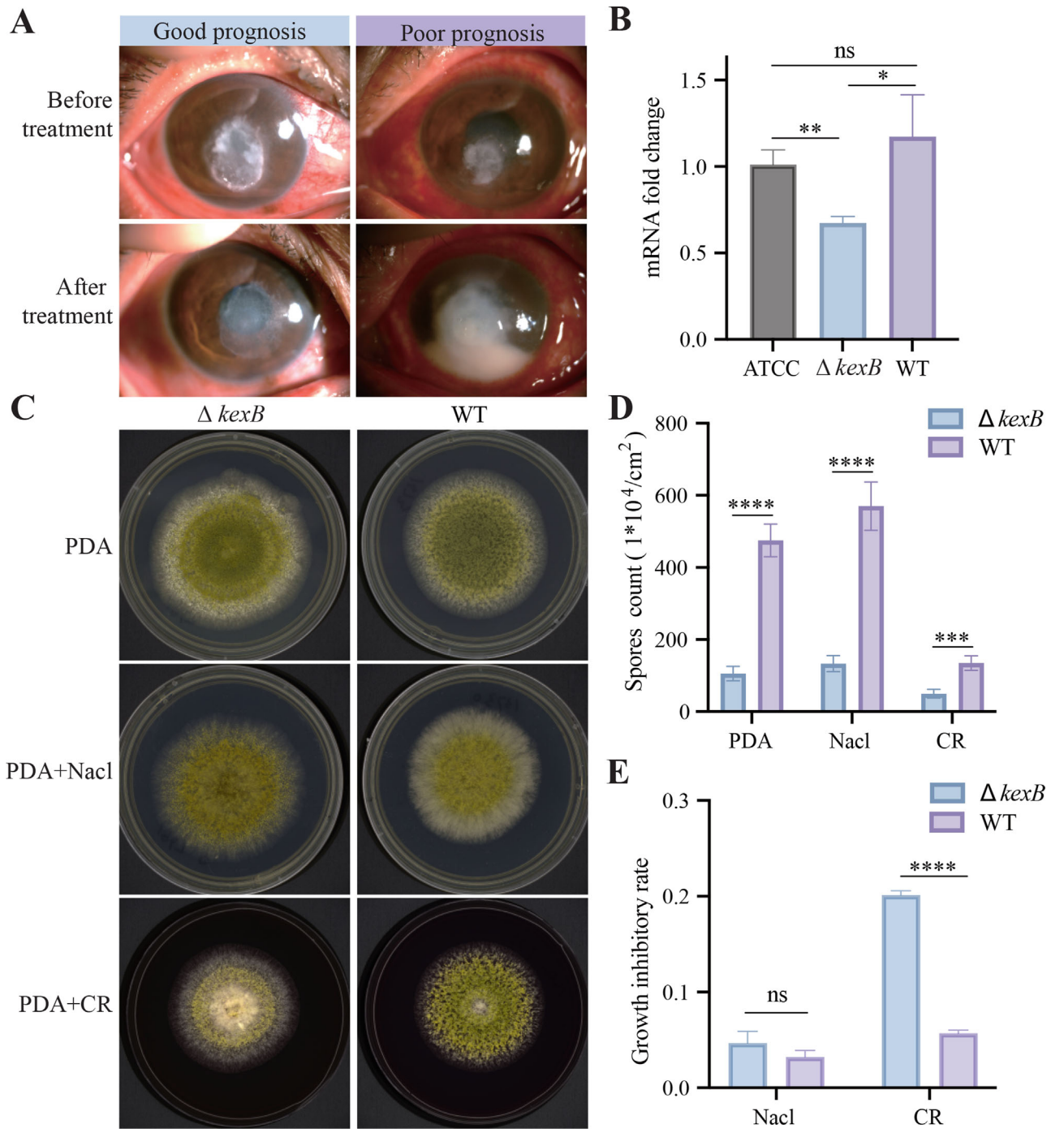

Figure 4. Growth phenotypes and sensitivity to cell wall perturbing compounds of the Δ*kexB*. (**A**) Representative anterior segment photographs of patients with *A. flavus* keratitis. (**B**) Decreased mRNA expression of the *kexB* gene in the Δ*kexB* mutant strains. (**C**) The isolated Δ*kexB* and WT strains grew on PDA media, with 1 mol/L NaCl and 100 µg/mL Congo Red at 5 days, respectively. (**D**) Conidia counting of the Δ*kexB* and WT at 28°C. (**E**) The growth inhibitory rate between two groups. ****$P < 0.0001$, ***$P < 0.001$, **$P < 0.01$, *$P < 0.05$; ns, not significant.

proteolysis, metallopeptidase activity, peptidase activity, etc (Fig. 3D).

Growth Phenotypes of the Δ*kexB* Strains. Compared with the ATCC strain, the mean mRNA expression levels of *kexB* gene decreased significantly in Δ*kexB* strains, while there was no obvious change in the WT strains, which was 0.67 folds ($P = 0.003$) and 1.17 folds ($P = 0.340$), respectively (Fig. 4B). In order to identify the microbiological features between the Δ*kexB* strains and the WT strains, we inoculated them on PDA agar medium for 5 days (Fig. 4C). The diameter of the colony was measured, which showed that there was little difference of colony morphology between the two groups when they grew on PDA media. To understand the strain's response to environmental stress, we tested fungal sensitivity to hyperosmotic stress factors and cell wall damaging agents. The number

Investigative Ophthalmology & Visual Science

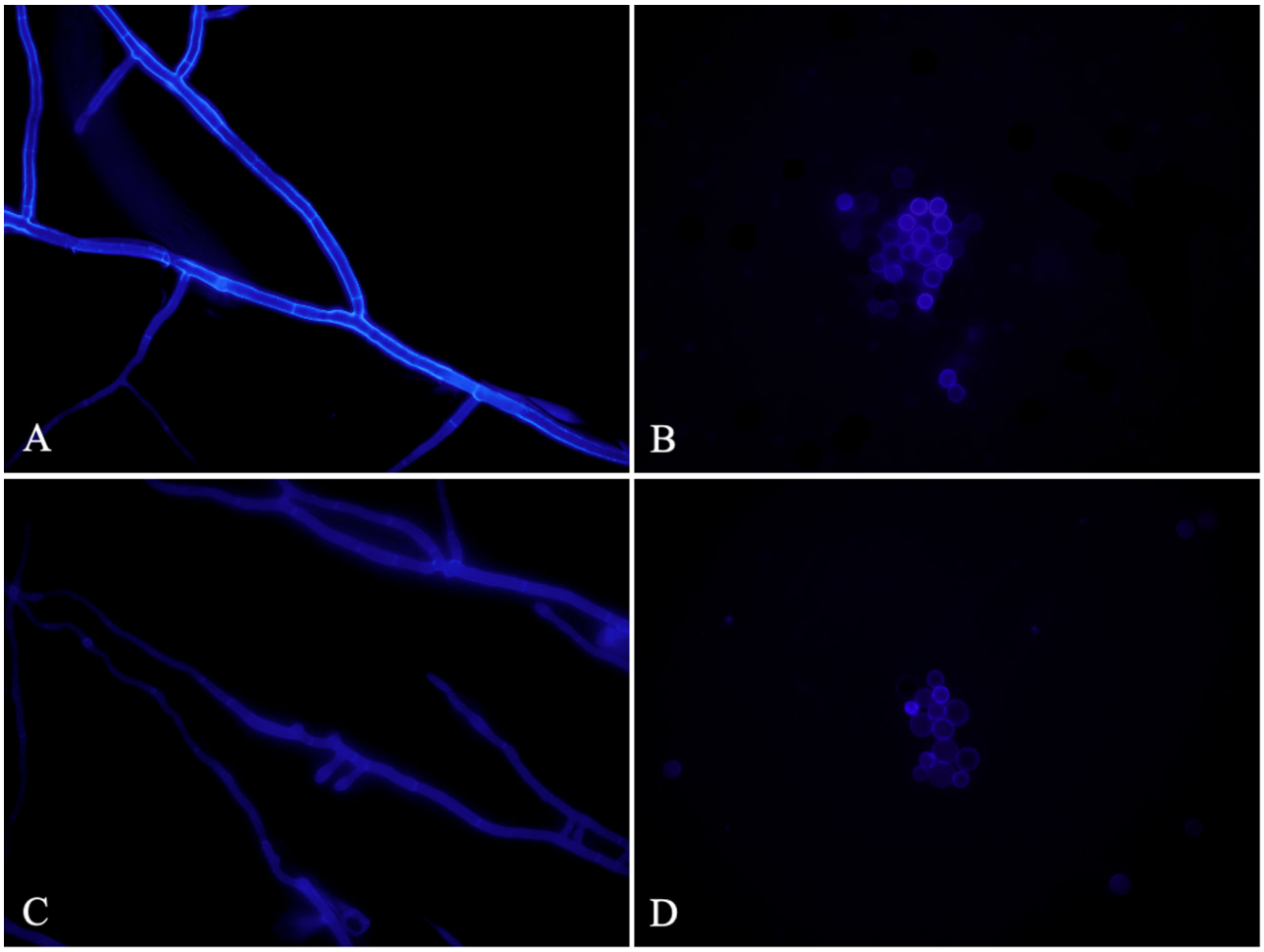

Figure 5. Fluorescent microphotographs of calcofluor white stained hyphae and conidia. (**A**, **B**) WT strains; and (**C**, **D**) Δ*kexB* mutant strains.

of spores, colony diameter, and growth inhibitory rate of the strains in the presence of the osmotic stress agents NaCl and cell-wall perturbing agents Congo red were analyzed. Conidia counting showed that the Δ*kexB* strains exhibited a remarkably reduced conidiation at 28°C when compared to the WT strains (Fig. 4D). The mean number of spores in the mutant and WT strains were 475.0/cm^2 and 105.8/cm^2 ($P <$ 0.0001), 570.0/cm^2 and 133.3/cm^2 ($P < 0.0001$), 134.8/cm^2 and 49.8/cm^2 ($P = 0.0004$) in PDA, and NaCl and Congo Red media, respectively. Interestingly, the Δ*kexB* strains also showed higher sensitivities to hyper osmotic stress (1 mol/L NaCl) and cell wall damaging agents (Fig. 4E). Compared to growth in PDA medium alone at 28°C, the growth of Δ*kexB* strains in the presence of 1 mol/L NaCl decreased by 4.6%, whereas the growth of strains from WT type decreased by 3.2% ($P = 0.343$). Similarly, cell wall stress imposed by the addition of 100 µg/mL Congo Red to the medium inhibited the growth of both strains. At 28°C, compared to growth in PDA medium alone, the growth rates of the Δ*kexB* strains and WT strains were significantly lower (by 20.1% and 5.7%, respectively, $P < 0.0001$).

Calcofluor White Staining of Wild-Type and Δ*kexB* Mutant Strain. Fluorescence microscopic examination of the WT and Δ*kexB* mutant strains following calcofluor white staining demonstrated that the fluorescence intensity of the Δ*kexB* mutant strain was distinctly lower than that of the WT strain (Fig. 5). The hyphae and spores of the WT strain presented a vivid bright blue fluorescence, whereas those of the Δ*kexB* mutant strain only showed a pale light blue.

Virulence of the Δ*kexB* Mutant Strains on Mice Cornea Infection. To validate the potential virulence effect of Δ*kexB* strains on corneal infection, intrastromal injections of 5000 conidia from the Δ*kexB* strains or WT strains were performed in the corneal stroma of C57BL/6 mice. Photographs of corneal ulcers with and without 1% sodium fluorescein were conducted on day 1, day 3, and day 5 after infection (Fig. 6A). On the first day, the mice inoculated with the mutant strain showed less severe corneal ulceration and a significantly lower clinical score (2.3 ± 1.0) compared to those with the WT strains (5.0 ± 0.8, $P = 0.005$; Fig. 6B). Regarding the outcome of *A. flavus* keratitis, the clinical scores of mice inoculated with the mutant strains were lower than those with the WT strains, which were 4.5 ± 2.6 and 8.7 ± 1.0, respectively ($P = 0.023$). The analysis of the corneal survival rate showed that, after 3 days, 80.0% (8/10) of the corneas infected with WT strains showed descemetocele or corneal perforation, which was significantly higher than those inoculated with the mutant strains (4/10, 40.0%). In addition, the log rank (Mantel-Cox) test showed that the survival curves were significantly different ($P < 0.0001$, Fig. 6C).

Investigative Ophthalmology & Visual Science

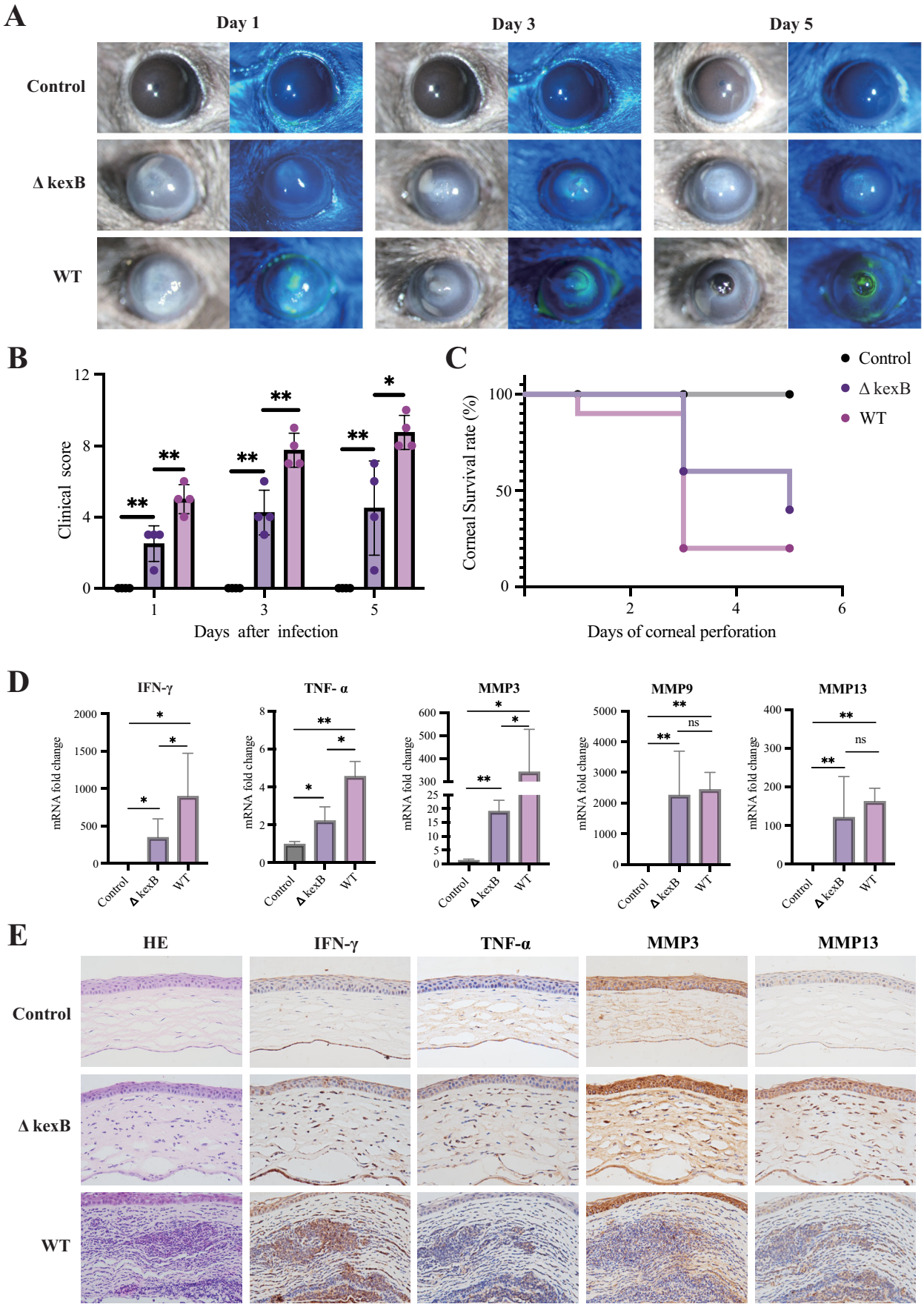

Figure 6. The *A. flavus* keratitis model mice infected by Δ*kexB* and WT strains. (**A**) The representative anterior segment photographs with and without fluorescein staining under slit lamp microscopy on days 1, 3, and 5 ($n = 4$). (**B**) The clinical scores and (**C**) corneal

Investigative Ophthalmology & Visual Science

survival rate was assessed in each group, and four mice were assessed in each group for the indicated time ($n = 4$). (**D**) Decreased gene expression of IFN-γ, TNF-α, MMP3, MMP9, and MMP13 in the mutant group. (**E**) H&E staining revealed a reduction in inflammatory cells and IHC showed decreased protein levels of IFN-γ, TNF-α, MMP3, and MMP13 in cornea tissues of the Δ*kexB* mutant group. ****$P < 0.0001$, ***$P < 0.001$, **$P < 0.01$, *$P < 0.05$; ns, not significant.

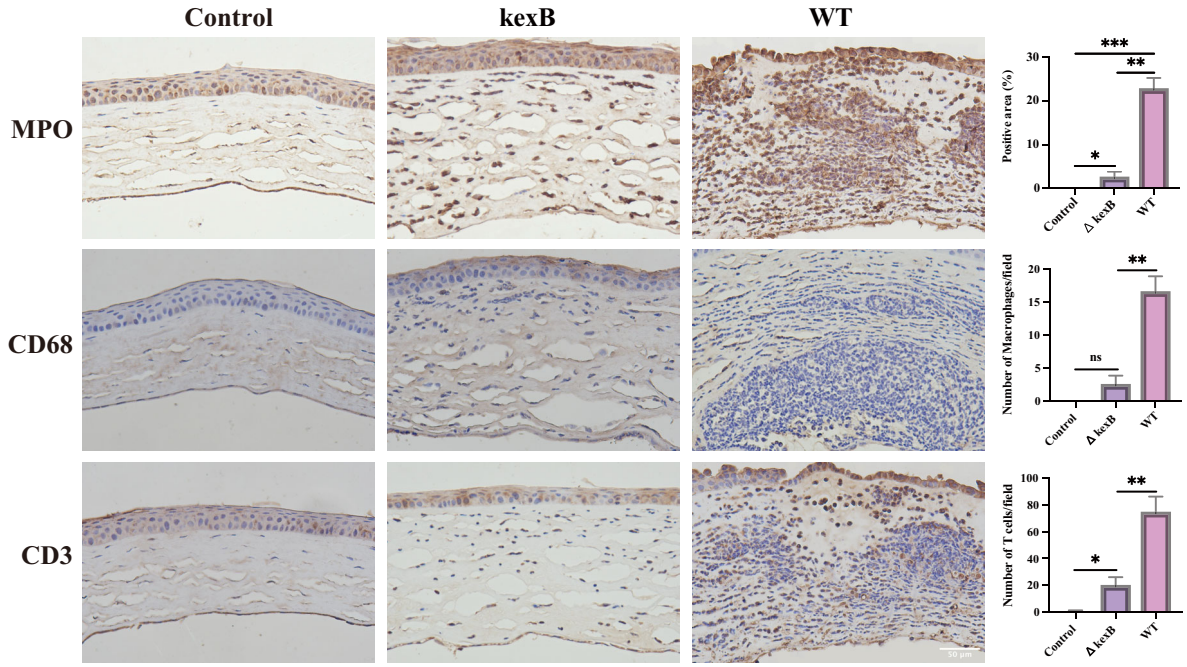

Figure 7. Infiltration of immune cells in mice cornea. Representative sections and quantitative analysis of the WT and Δ*kexB* mutant strains-infected corneas immune-stained with antibodies to neutrophils (MPO), macrophages (CD68), and T cells (CD3). ***$P < 0.001$, **$P < 0.01$, *$P < 0.05$; ns, not significant. Scale bar = 50 µm.

Compared with the WT group, hematoxylin and eosin (H&E) staining showed decreased infiltrated inflammatory cells in the mutant group. Concurrently, the mutant group exhibited significantly lower mRNA expression levels of IFN-γ, TNF-α, and MMP3, which was consistent with the outcomes of histological examination and clinical manifestations (all $P < 0.05$; Figs. 6D, 6E). To further investigate the infiltration of immune cells, tissue sections were immunostained with MPO, CD68, and CD3 antibodies to examine neutrophils, macrophages, and T cells, respectively. Our results revealed that the WT strains of *A. flavus* induced a significantly greater infiltration of neutrophils, macrophages, and T cells compared with the Δ*kexB* strains (all $P < 0.05$; Fig. 7). These data indicated that the Δ*kexB* strains alleviated the inflammation and stromatolysis of the infected cornea, highlighting their potential role in modulating the host immune response and corneal tissue damage.

Discussion

In this study, we investigated 21 cases of *A. flavus* keratitis and found that the clinical presentations and outcomes were notably variable, although there were no significant differences in MIC among *A. flavus* strains. Subsequently, pan-genome analysis revealed variations in the proportions of certain gene families among different strains. Further virulence gene analysis identified the *kexB* gene, which encoded a protein involved in cell wall glycan synthesis and was associated with the severity of keratitis. Mutations in this gene led to reduced conidia formation and higher sensitivity to cell wall damaging agents. Moreover, the mice models of *A. flavus* keratitis were established to validate the potential virulence effect of the Δ*kexB* strains through clinical scoring and immunohistochemistry. The results showed that Δ*kexB* strains caused significantly less inflammation and stromal melting compared with the WT strains. Our research uniquely linked *A. flavus* genomic features to clinical outcomes, providing novel insights into the pathogenicity of this fungus.

In this cohort, *A. flavus* keratitis exhibited poorer outcomes compared with other forms of fungal or infectious keratitis, which is consistent with previous cohorts of *A. flavus* keratitis.[3] Louisa et al. investigated the relationship between in vitro susceptibility and clinical outcomes in fungal keratitis, which revealed that a higher voriconazole MIC was correlated with an increased need for therapeutic penetrating keratoplasty among Fusarium-positive cases, but no significant correlations were observed among *Aspergillus* cases.[33] In this study, no relationships between antifungal susceptibility and treatment outcomes were found in *A. flavus*, consistent with the findings of Venkatesh et al.[34] According to clinical breakpoints, the voriconazole MIC for

Investigative Ophthalmology & Visual Science

all *A. flavus* isolates in our study were at or below the threshold of 1 µg/mL.[35] The same trend can be observed for Posaconazole, Itraconazole, and Amphotericin B, with clinical breakpoints of 0.5 µg/mL, 1 µg/mL, and 4 µg/mL, respectively.[19,36] These findings suggested that in vitro antifungal susceptibility testing may be not sufficient to predict treatment outcomes for *A. flavus* keratitis, underlining the need for further research to better understand their complex relationship.

Despite leading to diverse prognoses among patients, the strains did not exhibit prominent differences on the phylogenetic tree. The possible explanations could be as follows: although the whole genome contains abundant genetic information, the key gene regions that determine the pathogenicity and prognostic differences of strains during the infection process may only account for a small part of it. Meanwhile, their signals in the whole genome may be masked by the information of other non-key genes. Moreover, even though the variations in the whole genome may affect the biological behaviors of strains in a rather complex way, these differences are difficult to be directly reflected in the phylogenetic tree. The pan-genome analysis focused on the collective set of genes across all strains and revealed that the pan-genome of *A. flavus* was in a "closed" state.[37] This implies that the number of pan-genes did not substantially increase, indicating that a sufficient sample size was utilized to capture the overall genomic diversity of the *A. flavus* species. The functional distribution among the COG of *A. flavus* isolated from different clinical contexts suggested that certain categories may be highly associated with its pathogenicity.[38] Notably, within the core and accessory genomes of *A. flavus*, the gene cluster associated with the cell wall, membrane, and envelope biogenesis (category M) showed significant differences between strains isolated from patients with favorable and unfavorable outcomes.

Virulence genes involved in stress resistance, high growth rate, and nutritional versatility render *A. flavus* the primary pathogenic mold in fungal keratitis. Among these genes, the *kexB* gene, which encodes a kexin-like protein, has been proven to have crucial effects on cell wall integrity and virulence in multiple species including *Aspergillus* oryzae, Candida glabrata, and Candida albicans.[39,40] In this study, the *kexB* gene was identified in *A. flavus*, with a higher proportion of mutants observed in the group with good prognosis. Further experiments revealed that the Δ*kexB* resulted in the lower mRNA expression of *kexB*, and the mutant strains showed a reduced conidia formation as well as higher sensitivity to cell wall perturbing agents, which was in accordance with previous studies. Wang et al. demonstrated that the deletion of the *kexB* gene resulted in impaired N-glycan processing, and the activation of the MpkA-dependent cell wall integrity signaling pathway, which further resulted in a retarded growth, reduced conidia formation, temperature-sensitive defect in cell wall integrity, and attenuated virulence.[39]

Calcofluor white stain of *A. flavus* showed that fluorescence was much more intense in the WT strain than in the Δ*kexB* strain. This disparity indicates that the Δ*kexB* mutant strain has a reduced content of chitin and cellulose in its cell wall. This is further supported by the fact that calcofluor white can specifically bind to these components, which are crucial constituents of the cell wall structure.[41] Under the current experimental conditions, the *kexB* gene does not appear to have a direct influence on the drug sensitivity profile of *A. flavus* strains as all strains had MIC values within the clinical breakpoints.

The phenotypes of *A. flavus* keratitis corresponded to genotype-based groupings of *A. flavus* strains isolated from the patients. In the group with mutant strains, *A. flavus* keratitis was milder and showed relatively slow progression. In contrast, the group with WT strains presented with an acute onset on day 1 and exacerbated in the following days, leading to central corneal thinning and perforation in most of the mice models. Compared to the control group, H&E staining revealed more inflammatory cell activation in the lesion area. Furthermore, the relative mRNA expression level of inflammatory cytokines and matrix metalloproteinases also reflected the exacerbation of inflammation condition. Former research has indicated that much of the corneal destruction in microbial keratitis was likely due to an excessive host inflammatory response. Activated neutrophils attempt to destroy the pathogen through the production of reactive oxygen species and the release of enzymes such as MMPs but these mechanisms can also damage surrounding host tissue.[42,43] In our study, it was observed that after the injection of *A. flavus*, a substantial number of neutrophils were promptly recruited and rapidly amassed at the site of infection. Meanwhile, a limited quantity of T cells was detected infiltrating the area. Although their presence was not as conspicuous as that of the neutrophils, the engagement of T cells implies the initiation of the adaptive immune response. In comparison with the Δ*kexB* strains, the WT strains of *A. flavus* elicited a remarkably enhanced infiltration of neutrophils and macrophages, as well as T cells. Thus, *A. flavus* infection triggers the acute infiltration of immune cells in the cornea, further causing excessive inflammatory response and MMP, which resulted in cornea opacification, corneal thinning, and even perforation.

Through gene interaction and functional enrichment analysis, we discovered that the *kexB* gene network was mainly related to proteolytic activity. As secretory proteins are important virulence factors for fungi to overcome the host defense and propagate in the cornea, the downregulation of *kexB* gene in the mutant strain may affect the function of this network and lead to defect in conidia formation, and cell wall integrity, as well as invasion, thus resulting in a slower course of infection, a milder inflammatory response, and less tissue damage.[44]

Our study still had several limitations. First, due to the limited sample size, this study primarily explored the role of *kexB* gene mutation. Nevertheless, incorporating a larger cohort could identify additional virulence factors associated with the severity of keratitis. Second, we mainly focused on the phenotypic characteristics of the strains, the mechanism regarding how the *kexB* gene affected the host-pathogen interaction requires further research. Finally, the bioinformatics methods were mainly used to investigate the role of the *kexB* gene in the regulatory network. Although the algorithms of these methods have been proven accurate and reliable, it would be more beneficial to validate in vivo at the nucleic acid levels using molecular biological techniques.

In summary, our study correlates the genomic characteristics of *A. flavus* with clinical manifestations, providing a novel perspective for an in-depth understanding of the pathogenicity of *A. flavus*. The *kexB* gene holds promise as a new target for the diagnosis and treatment of *A. flavus* keratitis. Future studies can further explore the interactions between the *kexB* gene and other virulence genes, as well

as the impact of different host immune responses on *kexB* gene mutations.

Acknowledgments

Supported by the National Key Research and Development Program, grant number 2021YFC2301000.

Author Contributions: J. Liu, M. Kang, J. Pang, and Y. Wei performed the experiments. J. Liu analyzed the data and wrote the manuscript. Z. Zhang and X. Xu performed the bioinformatics analysis. M. Kang revised the manuscript. Yang Zhang, Kexin Chen, Zhiqun Wang, and Xinxin Lu provided materials. Q. Liang designed the experiment, provided materials, and revised the paper. All authors read and approved the final manuscript. All authors have read and agreed to the published version of the manuscript.

Disclosure: **J. Liu**, None; **M. Kang**, None; **Y. Wei**, None; **Z. Zhang**, None; **J. Pang**, None; **Q. Chen**, None; **X. Xu**, None; **Z. Wei**, None; **Y. Zhang**, None; **K. Chen**, None; **Z. Wang**, None; **X. Lu**, None; **Q. Liang**, None

References

1. Brown L, Leck AK, Gichangi M, Burton MJ, Denning DW. The global incidence and diagnosis of fungal keratitis. *Lancet Infect Dis*. 2021;21(3):e49–e57.
2. Kanaujia R, Singh S, Rudramurthy SM. Aspergillosis: an update on clinical spectrum, diagnostic schemes, and management. *Curr Fungal Infect Rep*. 2023;17(2):144–155.
3. Al-Hatmi AMS, Castro MA, De Hoog GS, et al. Epidemiology of Aspergillus species causing keratitis in Mexico. *Mycoses*. 2019;62(2):144–151.
4. Erdem E, Yagmur M, Boral H, Ilkit M, Ersoz R, Seyedmousavi S. Aspergillus flavus keratitis: experience of a tertiary eye clinic in Turkey. *Mycopathologia*. 2017;182(3-4):379–385.
5. Manikandan P, Varga J, Kocsubé S, et al. Epidemiology of Aspergillus keratitis at a tertiary care eye hospital in South India and antifungal susceptibilities of the causative agents. *Mycoses*. 2013;56(1):26–33.
6. Liu J, Wei Z, Cao K, Zhang Z, Xu X, Liang Q. Trends of ocular fungal infections in North China (2001–2020). *J Infect Public Health*. 2023;16(1):71–77.
7. Hatmaker EA, Rangel-Grimaldo M, Raja HA, et al. Genomic and phenotypic trait variation of the opportunistic human pathogen aspergillus flavus and its close relatives. Alanio A, ed. *Microbiol Spectr*. 2022;10(6):e03069–e03122.
8. Barber AE, Sae-Ong T, Kang K, et al. Aspergillus fumigatus pan-genome analysis identifies genetic variants associated with human infection. *Nat Microbiol*. 2021;6(12):1526–1536.
9. Amaike S, Affeldt KJ, Yin WB, Franke S, Choithani A, Keller NP. The bZIP protein MeaB mediates virulence attributes in Aspergillus flavus. Harris S, ed. *PLoS One*. 2013;8(9):e74030.
10. Jahn B, Boukhallouk F, Lotz J, Langfelder K, Wanner G, Brakhage AA. Interaction of human phagocytes with pigmentless Aspergillus Conidia. Kozel TR, ed. *Infect Immun*. 2000;68(6):3736–3739.
11. Zhang Y, Wang Y, Fan J, Zhu G, Lu L. Aspergillus fumigatus Elongator complex subunit 3 affects hyphal growth, adhesion and virulence through wobble uridine tRNA modification. Andrianopoulos A, ed. *PLoS Pathog*. 2022;18(11):e1010976.
12. Yuan J, Li D, Qin L, et al. HexA is required for growth, aflatoxin biosynthesis and virulence in Aspergillus flavus. *BMC Mol Biol*. 2019;20(1):4.
13. Barakat GII, Kamal YN, Sultan AM. Could aflatoxin B1 production by Aspergillus flavus affect the severity of keratitis: an experience in two tertiary health care centers, Egypt. *Eur J Clin Microbiol Infect Dis*. 2019;38(11):2021–2027.
14. Gangurde SS, Korani W, Bajaj P, et al. Aspergillus flavus pangenome (AflaPan) uncovers novel aflatoxin and secondary metabolite associated gene clusters. *BMC Plant Biol*. 2024;24(1):354.
15. Acharya M, Farooqui JH, Jain S, Mathur U. Pearls and paradigms in infective keratitis. *Romanian J Ophthalmol*. 2019;63(2):119–127.
16. Wang HC, Hsieh MI, Choi PC, Wu CJ. Comparison of the Sensititre YeastOne and CLSI M38-A2 microdilution methods in determining the activity of amphotericin B, itraconazole, voriconazole, and posaconazole against Aspergillus Species. Warnock DW, ed. *J Clin Microbiol*. 2018;56(10):e00780–e00818.
17. Korkmaz E, Ergon MC. Investigation of antifungal susceptibility of Aspergillus species isolated from systemic clinical specimens by different methods. *Indian J Med Microbiol*. 2024;50:100642.
18. Clinical and Laboratory Standard Institute (CLSI). *Reference Method for Broth Dilution Antifungal Susceptibility Testing of Filamentous Fungi*. 3rd ed. CLSI standard M38. Wayne, PA: Clinical and Laboratory Standards Institute; 2017.
19. Lamoth F, Alexander BD. Comparing etest and broth microdilution for antifungal susceptibility testing of the most-relevant pathogenic molds. *J Clin Microbiol*. 2015;53(10):3176–3181.
20. Espinel-Ingroff A, Rezusta A. E-test method for testing susceptibilities of Aspergillus spp. to the new triazoles voriconazole and posaconazole and to established antifungal agents: comparison with NCCLS broth microdilution method. *J Clin Microbiol*. 2002;40(6):2101–2107.
21. Gurevich A, Saveliev V, Vyahhi N, Tesler G. QUAST: quality assessment tool for genome assemblies. *Bioinformatics*. 2013;29(8):1072–1075.
22. Rawlings ND, Barrett AJ, Thomas PD, Huang X, Bateman A, Finn RD. The MEROPS database of proteolytic enzymes, their substrates and inhibitors in 2017 and a comparison with peptidases in the PANTHER database. *Nucleic Acids Res*. 2018;46:D624–D632.
23. Zheng J, Ge Q, Yan Y, Zhang X, Huang L, Yin Y. dbCAN3: automated carbohydrate-active enzyme and substrate annotation. *Nucleic Acids Res*. 2023;51(W1):W115–W121.
24. Seppey M, Manni M, Zdobnov EM. BUSCO: assessing genome assembly and annotation completeness. In: Kollmar M, ed. *Gene Prediction*. Vol. 1962. Methods in Molecular Biology. New York, NY: Springer; 2019:227–245.
25. Finn RD, Attwood TK, Babbitt PC, et al. InterPro in 2017—beyond protein family and domain annotations. *Nucleic Acids Res*. 2017;45(D1):D190–D199.
26. Chaudhari NM, Gupta VK, Dutta C. BPGA - an ultra-fast pan-genome analysis pipeline. *Sci Rep*. 2016;6(1):24373.
27. Tatusov RL. The COG database: new developments in phylogenetic classification of proteins from complete genomes. *Nucleic Acids Res*. 2001;29(1):22–28.
28. Buchfink B, Xie C, Huson DH. Fast and sensitive protein alignment using DIAMOND. *Nat Methods*. 2015;12(1):59–60.
29. Urban M, Cuzick A, Seager J, et al. PHI-base in 2022: a multi-species phenotype database for pathogen–host interactions. *Nucleic Acids Res*. 2022;50(D1):D837–D847.
30. Szklarczyk D, Gable AL, Lyon D, et al. STRING v11: protein–protein association networks with increased coverage, supporting functional discovery in genome-wide experimental datasets. *Nucleic Acids Res*. 2019;47(D1):D607–D613.
31. Xu X, Wei Y, Pang J, et al. Time-course transcriptomic analysis reveals the crucial roles of PANoptosis in fungal keratitis. *Invest Opthalmol Vis Sci*. 2023;64(3):6.

32. Wu TG, Wilhelmus KR, Mitchell BM. Experimental keratomycosis in a mouse model. *Invest Opthalmol Vis Sci*. 2003;44(1):210.
33. Lu L, Prajna NV, Lalitha P, et al. Association between in vitro susceptibility and clinical outcomes in fungal keratitis. *J Ophthalmic Inflamm Infect*. 2024;14(1):42.
34. Prajna VN, Lalitha PS, Mascarenhas J, et al. Natamycin and voriconazole in Fusarium and Aspergillus keratitis: subgroup analysis of a randomised controlled trial. *Br J Ophthalmol*. 2012;96(11):1440–1441.
35. Sun CQ, Lalitha P, Prajna NV, et al. Association between in vitro susceptibility to natamycin and voriconazole and clinical outcomes in fungal keratitis. *Ophthalmology*. 2014;121(8):1495–1500.e1.
36. Arendrup MC, Cuenca-Estrella M, Lass-Flörl C, Hope WW. EUCAST technical note on Aspergillus and amphotericin B, itraconazole, and posaconazole. *Clin Microbiol Infect*. 2012;18(7):E248–E250.
37. Liu Y, Du H, Li P, et al. Pan-genome of wild and cultivated soybeans. *Cell*. 2020;182(1):162–176.e13.
38. Ling X, Gu X, Shen Y, et al. Comparative genomic analysis of Acanthamoeba from different sources andhorizontal transfer events of antimicrobial resistance genes. Ralston KS, ed. *mSphere*. Available at: https://journals.asm.org/doi/10.1128/msphere.00548-24.
39. Wang J, Zhou H, Lu H, et al. Kexin-like endoprotease KexB is required for N-glycan processing, morphogenesis and virulence in Aspergillus fumigatus. *Fungal Genet Biol*. 2015;76:57–69.
40. Bader O, Schaller M, Klein S, et al. The *KEX2* gene of Candida glabrata is required for cell surface integrity. *Mol Microbiol*. 2001;41(6):1431–1444.
41. Rudhra O, Gnanam H, Sivaperumal S, Namperumalsamy V, Prajna L, Kuppamuthu D. Melanin depletion affects Aspergillus flavus conidial surface proteins, architecture, and virulence. *Appl Microbiol Biotechnol*. 2024;108(1):291.
42. Chidambaram JD, Kannambath S, Srikanthi P, et al. Persistence of innate immune pathways in late stage human bacterial and fungal keratitis: results from a comparative transcriptome analysis. *Front Cell Infect Microbiol*. 2017;7:193.
43. Karthikeyan RS, Leal SM, Prajna NV, et al. Expression of innate and adaptive immune mediators in human corneal tissue infected with aspergillus or fusarium. *J Infect Dis*. 2011;204(6):942–950.
44. Selvam RM, Nithya R, Devi PN, et al. Exoproteome of Aspergillus flavus corneal isolates and saprophytes: identification of proteoforms of an oversecreted alkaline protease. *J Proteomics*. 2015;115:23–35.